

Properties of MIM AISI 420 via Pre-alloyed and Master Alloy Routes

Andrew J Coleman, Keith Murray, Martin Kearns, Toby A. Tingskog*,
Bob Sanford** & Erainy Gonzalez**

Sandvik Osprey Ltd., Red Jacket Works, Milland Road, Neath, SA11 1NJ, UK

*Sandvik Osprey Ltd., USA

** TCK S.A., Zona Franca Industrial Las Americas, Santo Domingo, Dominican Republic

ABSTRACT

AISI 420 is a hardenable, martensitic stainless steel widely used in the MIM industry for applications where high hardness and wear resistance are required along with some corrosion resistance. These characteristics mean that the alloy is often used in the automotive sector and for the production of parts for firearms and power tool components as well as surgical instruments. Its popularity has been achieved in spite of the difficulties faced in controlling sintering in a relatively narrow process window.

In this study we look at the effect of particle size distribution on as-sintered and heat-treated properties of components made with pre-alloyed powder. These are compared with properties obtained from parts produced using a master alloy and carbonyl iron powder blend. Tensile properties are reported for samples sintered at different temperatures and metallographic analysis was performed on as sintered and heat treated samples.

INTRODUCTION

420 stainless steel is one of the basic martensitic stainless steels with a composition of Cr 12.0-14.0% and C 0.15% min with Fe balance. The carbon level is not limited in the specification but generally does not exceed 0.4%. Typically carbon is controlled in the range 0.20-0.30% depending on the desired hardness. Higher carbon leads to increased hardness at the expense of ductility and corrosion performance.

There are a two ways to produce this alloy using different powder combinations: 1) Simply use Prealloyed (PA) powder of the desired composition, or 2) Blend Carbonyl Iron Powder (CIP) with a FeCr Master Alloy (MA) powder with a 4x concentration of Cr.

Previous work has demonstrated the benefits of using low alloy steel MAs over PA powder [1-3]. These include improved mechanical properties, better control of distortion, better control of chemistry and, potentially, cost advantages – particularly for low alloy steels.

In this study we evaluate the sintered properties of 420 made from both PA and MA+CIP routes as a function of sintering cycle and sintering atmosphere.

Published data for as sintered and heat treated MIM and wrought AISI 420 parts are shown in Table 1. These demonstrate the wide range of mechanical properties achievable from this alloy by heat treatment.

Table 1: Published values for AISI 420

Form & heat treatment	UTS MPa (ksi)	0.2%PS MPa (ksi)	%El	Density g/cm ³	Density %TD	UTS MPa (ksi)	0.2%PS MPa (ksi)	%El	Hardness HRC
Bar stock, annealed	586 (85)	276 (40)	25	7.74	-	-	-	-	88 HRB
Bar stock, hardened	1586 (230)	1344 (195)	8		-	-	-	-	55
420 (MPIF 35) Heat treated[7]	-	-	-	7.4	95	1380 (200)	1200 (174)	<1	44
420 (Parmatech) HIP & HT	-	-	-	7.7	99	1800	1500	3	52
German & Bose [4], Heat treated	-	-	-	-	92	1440	690	6	47

EXPERIMENTAL PROCEDURE

420 PA and MA powders were produced by Sandvik Osprey's proprietary inert gas atomisation process using nitrogen gas. All gas atomised powders were air classified to a particle size distribution of 90%-22µm. Carbonyl Iron Powders (CIP), containing either high (HC) or low carbon (BC), were obtained from Sintez. The chemistry of the powder batches used is shown in Table 2.

Table 2: Chemical analysis of powders used in this study, a) 420 powders and b) CIP

a)

Alloy	Fe	Cr	Mn	Si	C	P	S	O
420	Bal	13.1	0.74	0.67	0.28	0.011	0.005	0.068
420MA	Bal	49.4	1.7	1.5	0.01	-	-	-
420MA + CIP	Bal	12.5	0.6	0.6	0.35	0.005	0.004	-

b)

CIP grade	Fe	C	O	N
CIP HC	Bal	0.78	0.16	0.81
CIP BC	Bal	0.022	0.30	0.005

For both the PA and MA+CIP materials, feedstock was produced with carbon content meeting the carbon specification for AISI 420 of 0.15% C min.

The particle size distributions of the powders used in this study are shown in Table 3. The table also shows the Melt Flow Index for each feedstock. This confirms that the coarser PA feedstock has much lower viscosity than that made with MA+CIP.

Feedstocks were prepared at different powder loadings using TCKs proprietary binder. 420 MA+CIP feedstock was prepared with 17.4% shrinkage factor and the PA with a 16% shrinkage factor. The shrinkage factor is the scale factor applied to the target final part dimensions in order to design the mould.

The feedstocks were moulded in an Arburg injection moulding unit and sintered by TCK in an Elnik furnace, to produce standard MIMA tensile and Charpy test specimens.

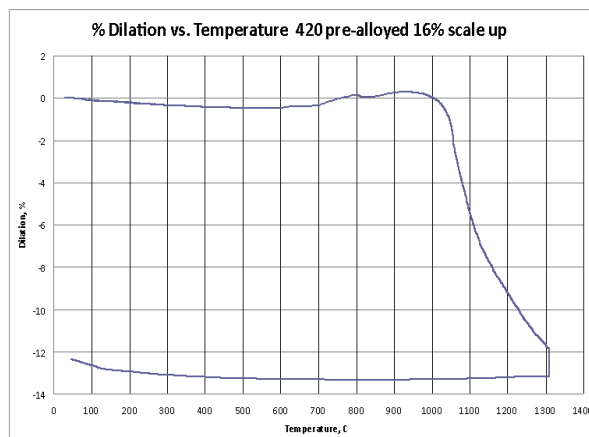
Table 3: Particle size & Melt Flow Index (MFI) data

Alloy	Particle Size (μm)	Particle Size Data (μm)			Shrinkage Factor (%)	MFR, g/min
		D90	D50	D10		
420 PA	90%-22 μm	20.7	9.7	3.7	16	232
420 MA	90%-22 μm	19.9	10.0	4.0		
CIP HC		10.6	5.1	2.6		
CIP BC		11.2	5.6	2.6		
MA + CIP	90%-14 μm	13.2	6.0	2.5	17.4	130

Sintering

Moulded green parts were subject to an initial solvent debind followed by a thermal debind at 500°C (932°F) and sintering in a nitrogen atmosphere, with the exception of run 3 which was sintered in hydrogen. Four different sintering cycles were run on a series of tensile and Charpy specimens after debinding. The sintering cycles were devised following a brief dilatometric study of the PA and MA+CIP feedstocks to examine their respective shrinkage behavior. For the PA feedstock, the fastest rate of shrinkage occurred at ~ 1075-1100°C and densification neared completion at ~ 1310°C – see Figure 1. The MA+CIP specimen showed a much earlier onset of gradual shrinkage without the steep decline shown in Figure 1. Cycles were run to examine the impact of holding periods in the temperature zone where the densification rate was greatest.

Figure 1: Dilatometry trace for 420PA in nitrogen



Run 1: 2°C/min ramp to 1075°C, 60 min hold, 2°C/min ramp to 1350°C, 60 min hold.

Run 2: 5°C/min ramp to 1350°C, 120 min hold.

Run 3: Like run 2 except with hydrogen atmosphere.

Run 4: 2°C/min ramp to 1100°C, 30 min hold, 5°C/min ramp to 1350°C, 120 min hold.

Sintered parts were allowed to slow cool under a nitrogen atmosphere. As sintered tensile samples were kept for triplicate testing and further samples were heat treated and tempered (solutionise for 1h at 1000°C followed by air quench and temper at 250°C for 1h). Tensile testing was carried out on three specimens in each condition in accordance with ASTM E8-08. Vickers hardness testing was carried out using a 10kg weight. Sintered density measurements were carried out using a Micromeritics Accupyc II1340 Helium Pycnometer. Polished cross-sections of Charpy bars were prepared for porosity measurements and

microstructures were analysed in the polished and etched (Vilella's reagent) conditions. In order to evaluate distortion during sintering, Charpy test bars were suspended across refractory supports, separated by 38mm in the sintering furnace. After sintering, the Charpy bars were taken for measurement and these results will be published in a subsequent paper.

RESULTS

As-sintered parts were analyzed for mechanical properties, hardness and C content. Table 4 shows the test values. Carbon analysis of as-sintered parts shows that carbon levels were well controlled for both the PA and MA variants sintered in nitrogen but significant carbon loss was observed in both PA and MA parts sintered in hydrogen.

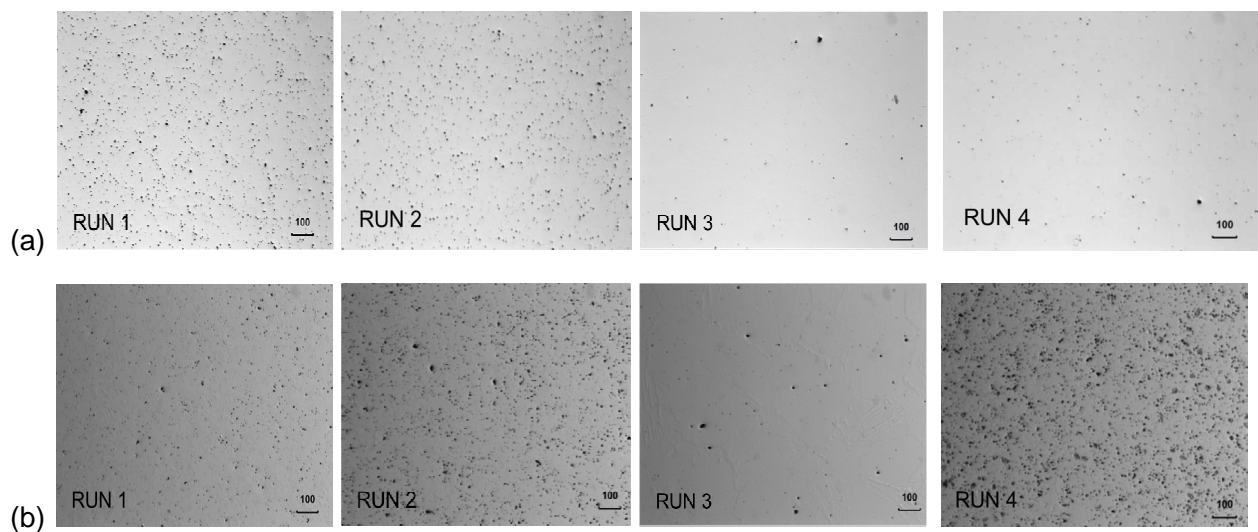
Table 4: Properties of as-sintered bars.

MA or PA	RUN	Atm	UTS, MPa	0.2%PS, MPa	%El.	Density, g/cm ³	Density, %TD	Hardness HRC	%C
MA	1	N2	1163-1465	594-628	1.5	7.16	92.8	48-51	0.42
MA	2	N2	1089-1159	571-666	1-2.5	7.3	94.2	50-52	0.42
MA	3	H2	381-406	187-202	24	7.65	98.8	116-137HV	0.02
MA	4	N2	1342-1351	636-686	1.5	7.21	93.5	46-48	0.35
PA	1	N2	723-779	593-622	1-1.5	7.25	93.9	50-51	0.27
PA	2	N2	749-813	608-639	-	7.29	94.5	46-49	0.28
PA	3	H2	771-913	487-907	1.5-3.5	7.52	97.2	45-49	0.17
PA	4	N2	762-775	580-583	1.5	7.25	93.9	47-49	0.26

Marginally higher sintered density was achieved in the PA parts vs the MA+CIP variants sintered in nitrogen. In the case of parts sintered in hydrogen, however, the MA+CIP parts achieved higher density than their PA counterparts but in both cases, significantly higher sintered density was achieved compared with the parts sintered in nitrogen.

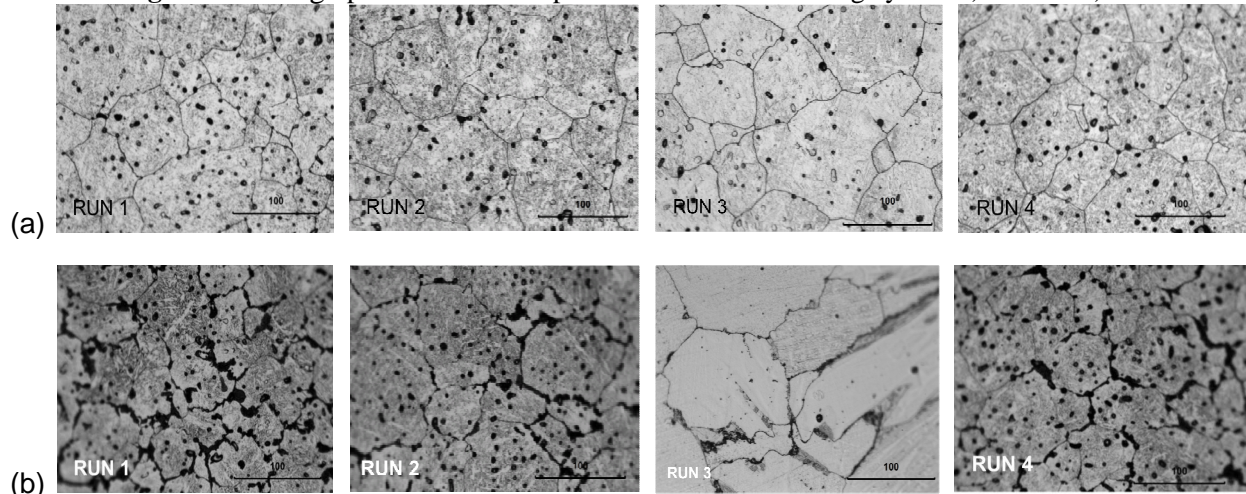
Metallographic analysis was carried out on samples from each sintering run and powder type. Images of the polished microstructures for the PA and MA variants are shown in Figure 2.

Figure 2: Micrographs of as-polished samples from the four sintering cycles: a) PA and b) MA



There is a good correlation between the apparent porosity level and the measured density for parts processed via cycles 1-3, but the low porosity apparent in sample 4 is at odds with both the measured density and the porosity observed in the etched sample (see Figure 3). For the MA+CIP samples, there is a strong correlation between the porosity apparent in micrographs and measured density for samples processed in all 4 sintering cycles.

Figure 3: Micrographs of etched samples from the four sintering cycles: a) PA and b) MA

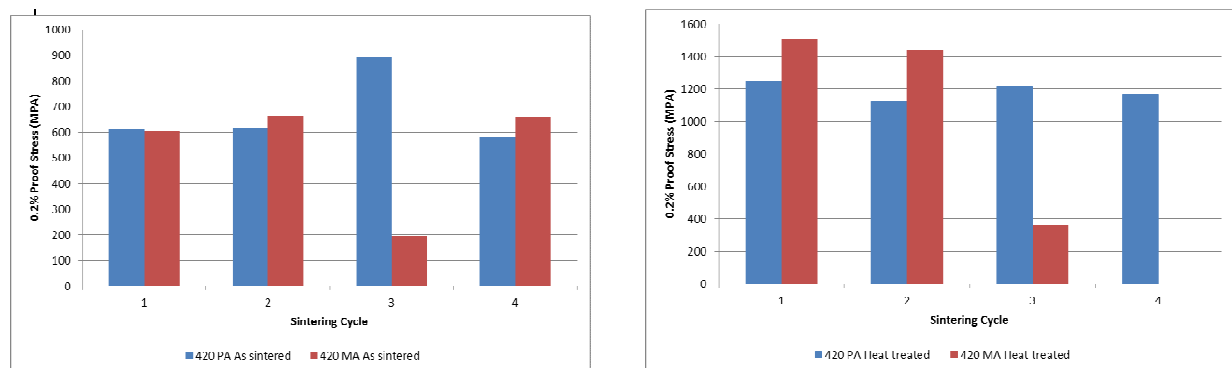


Examination of the sintered PA microstructures shows tempered martensite in all cases with fine chromium carbides dispersed throughout the matrix. The quantity of carbides in the hydrogen-sintered sample (run 3) is much lower than in the samples sintered in nitrogen reflecting the significant carbon loss that occurred during the run (see Table 4). Analysis of the MA+CIP samples sintered in nitrogen reveals the same martensitic structure observed in the PA samples, but in this case, coarse chromium carbides are concentrated primarily at grain boundaries. In the case of the hydrogen-sintered MA samples, the grain size is considerably coarser and only a small number of carbides are present, primarily at grain boundaries.

Mechanical Properties

Tensile tests were carried out on as-sintered (AS) and heat treated (HT) samples (no MA samples from cycle 4 were available for HT). Proof stress and tensile strength results are presented in Figures 4 and 5.

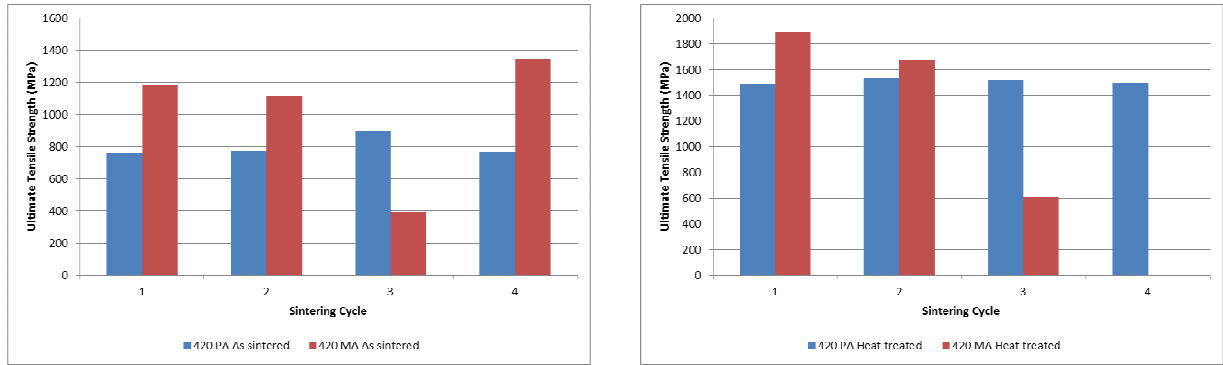
Figure 4: 0.2% Proof Stress for 420 PA & MA specimens in AS (left) & HT (right) condition



For materials sintered in nitrogen, proof stress values measured for the PA and MA+CIP specimens in the AS condition are quite consistent at ~600MPa. In the HT condition, proof stress of the PA is elevated to ~1200MPa and that of the MA+CIP samples is a further 2-300MPa higher again. For the hydrogen-sintered

specimens, significantly higher proof stress is seen for the PA in the AS condition, while the proof strength of the MA+CIP version has deteriorated. In the HT condition, the hydrogen-sintered PA shows a similar proof stress to the nitrogen-sintered PA but the MA+CIP properties are even more markedly depressed (350MPa).

Figure 5: UTS values for 420 PA & MA in the AS (left) & HT (right) conditions



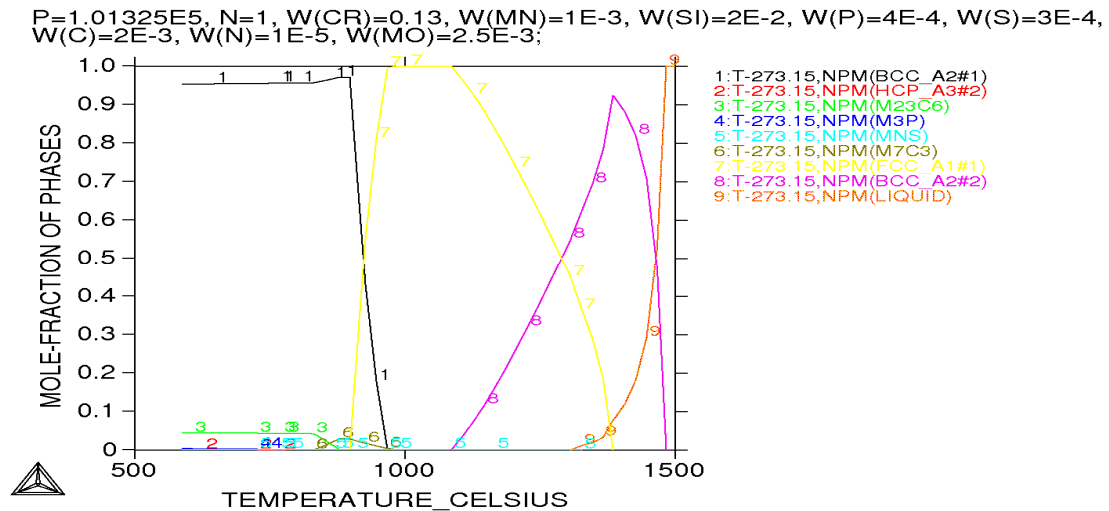
Examination of the data for the PA samples in Figure 5 confirms that the measured tensile strength results are quite consistent across all 4 sintering cycles in both the AS and HT condition. The MA+CIP variant, however, appears to be more sensitive to the sintering atmosphere used. The tensile strength results for the hydrogen-sintered samples are much lower than the nitrogen-sintered samples.

DISCUSSION

The sintering cycles chosen for these studies were intended to shed light on the influence of holding periods in a temperature range where the rate of densification of PA appears to be highest, and whether this would lead to higher final density. However, density data from samples sintered in cycles 1, 2 and 4 in nitrogen reveals little effect of the different holding periods on final density. In all cases, the density level achieved of 7.2 – 7.3 g cm⁻³ is similar to values reported elsewhere for conventional MIM 420 alloys. Higher density has been reported after HIPping and in 420 alloy variants that containing a small amount of Nb which is known to influence the amount of liquid phase present during sintering [5].

A ThermoCalc analysis of the 420 system with 13%Cr and 0.2%C is shown in Figure 6. The onset of shrinkage shown in Figure 1 coincides with the emergence of delta ferrite and as the temperature rises, so the

Figure 6: ThermoCalc analysis of the 420 system with 13%Cr and 0.2%C



volume fraction of delta ferrite increases. The presence of this phase is associated with increased densification in studies on 17-4PH [6] and it enables faster diffusion than the austenitic phase which dominates at lower temperature. At approximately 1380°C, delta phase reaches its maximum volume fraction of 90% and before this, at approximately 1330°C liquid phase begins to form. The volume fraction of liquid rises only slowly at first with rising temperature but as the temperature increases further, there is a greater risk of partial melting and distortion.

The complexity of the densification process is compounded by the interplay of interstitial elements in the powders with the sintering atmosphere which will affect final carbon level and therefore phase stability and onset of melting. Cycle 3 in hydrogen was successful in significantly increasing the density of both PA and MA samples but at the cost of much reduced C level, particularly in the case of the MA variant (Table 4). This is accompanied by significant coarsening in grain size (Figure 3) and, in the case of the MA+CIP variant, much reduced strength and hardness levels. Interestingly however, sintering in hydrogen leads to enhanced AS proof strength levels for the PA product. This is believed to be due to an increase in density outweighing the loss of carbon in contributing to strengthening mechanisms. The reduction of surface oxides by hydrogen enables densification to progress more rapidly.

The as-sintered proof strength properties are in line with the limited values shown in Table 1. The higher hardness and tensile strength values measured in AS MA+CIP vs PA specimens sintered in nitrogen may be related to a number of factors but one significant influence is the higher carbon level in the MA+CIP samples which are up to 0.15% higher (Table 4). The high UTS values displayed by the MA+CIP variants appear to be associated with high work hardening exponents connected with heavy grain boundary precipitation. The apparent gain in carbon after sintering the MA+CIP samples in nitrogen (Table 4) is not clear but the net result is high tensile strength in the AS and HT samples, in line with typical MPIF standard levels.

For the hydrogen-sintered samples, the MA + CIP variants exhibit lower strength levels than PA specimens and this correlates with the lower carbon levels measured in these samples. Carbon loss from the MA+CIP sample is far more pronounced than from the PA and this is believed to be due to carbon being present initially in fine CIP particles where diffusion will be more rapid than in the PA powder where carbon is homogeneously distributed in chromium rich carbides. When PA powder is sintered in hydrogen, carbon loss is significant and is encouraged by reduction of surface oxides by hydrogen followed by grain boundary diffusion of carbon. Table 4 confirms that carbon loss from PA samples sintered in nitrogen is minimal.

SUMMARY AND CONCLUSIONS

The present study confirms that achieving high density in 420-stainless steel is not straightforward. Controlled addition of hydrogen to a nitrogen sintering atmosphere offers some scope for the PA product, but in the MA+CIP variant, carbon loss in a hydrogen-rich atmosphere appears excessive. Carbon loss in hydrogen atmospheres leads to a dramatic reduction in strength levels but markedly improves densification and ductility. An optimised nitrogen/hydrogen sintering atmosphere should give the best combination of density, strength and ductility by control of grain boundary chemistry.

In nitrogen atmospheres, the MA+CIP route typically gives slightly higher density than PA (+1%) under equivalent sintering conditions (~94% vs 93%). MA+CIP variants generally show significantly higher UTS in the AS condition vs PA, though 0.2%PS values are similar. The high, AS UTS values shown by the MA+CIP product appears to be related to its distinctive grain boundary carbide structure.

The MA+CIP approach is shown to lead to higher tensile strength values than the PA route albeit the significant difference in final C level may well be the primary cause of this difference. The MA+CIP route can therefore offer advantages, but is more prone to variable carbon control if hydrogen atmospheres are used.

ACKNOWLEDGEMENTS

Thanks are due to Dr. Johan Sundstrom of Sandvik Materials Solutions for Thermocalc studies.

REFERENCES

1. T.A. Tingskog, G.J. Del Corso, M.L. Schmidt and D.T. Whychell, “ Diffusion of Alloying Elements During Sintering of MIM Master Alloys”, Advances in Powder Metallurgy & Particulate Materials – 2002. Proceedings of the 2002 International Conference on Powder Metallurgy & Particulate Materials, Part 10, 156
2. P.A. Davies, G.R. Dunstan, D.F. Heaney and T.J. Mueller, “Comparison of Master Alloy and Pre-Alloyed 316L Stainless Steel Powders For Metal Injection Molding (MIM)”, PM2TEC 2004 World Congress, MPIF, Chicago, IL.
3. A.J. Coleman, K. Murray, M.A. Kearns, T. A. Tingskog, B. Sanford, E. Gonzalez, “Effect of Particle Size Distribution on Processing and Properties of Metal Injection Moulded 4140 and 4340”, PowderMet 2011, San Francisco, CA
4. Injection Molding of Metals & Ceramics, R M German & A Bose MPIF, 1997
5. Catamold 420W Datasheet, BASF, May 2008.
6. K. Murray, A. J. Coleman, T. Tingskog & D. Whychell, “Effect of Particle Size Distribution on Processing & Properties of MIM 17-4PH, Int. J. Powder Metall., 47(4), 21-28, 2011.
7. Material Standards for Metal Injection Moulded Parts, MPIF Standard 35, 2007 Edition